Published in final edited form as:
Dev Dyn. 2014 July ; 243(7): 937–947. doi:10.1002/dvdy.24125.

Loss of Function of Mouse Pax-Interacting Protein 1-Associated Glutamate Rich Protein 1a (Pagr1a) Leads to Reduced Bmp2 Expression and Defects in Chorion and Amnion Development

Amit Kumar[1,‡], **Margaret Lualdi**[2], **Jadranka Loncarek**[1], **Young-Wook Cho**[3,4], **Ji-Eun Lee**[3], **Kai Ge**[3], and **Michael R. Kuehn**[1,*]

[1]Laboratory of Protein Dynamics and Signaling, National Cancer Institute, National Institutes of Health, Frederick, Maryland [2]Laboratory Animal Sciences Program, Leidos Biomedical Research, Inc., Frederick, Maryland [3]Laboratory of Endocrinology and Receptor Biology, National Institute of Diabetes and Digestive and Kidney Diseases, National Institutes of Health, Bethesda, Maryland [4]Korea Basic Science Institute Chuncheon Center, Chuncheon, Kangwon, Korea

Abstract

Background—Human PAX-Interacting Protein 1 (PAXIP1)-associated glutamate rich protein 1 (PAGR1, also known as PA1) originally was discovered as part of a complex containing PAXIP1 and histone H3K4 methyltransferases MLL3 and MLL4, suggesting a role in epigenetic gene regulation. Further in vitro studies suggested additional functions in DNA damage repair and transcription. However, in vivo analysis of PAGR1 function has been lacking.

Results—Here we show that expression of the cognate mouse gene *Pagr1a* is found predominately in the extraembryonic and chorionic ectoderm from pregastrulation stages and is up-regulated within the embryo proper after gastrulation. Embryos with a germ line deletion of *Pagr1a* establish the anterior–posterior axis, and show normal neuroectodermal, mesodermal, and endodermal patterning, but fail to develop beyond the four- to five-somite stage or to undergo axial rotation. *Pagr1a*$^{-/-}$ embryos also show abnormal development of extraembryonic tissues with defects seen in the amnion, chorion and visceral yolk sac. At the molecular level, *Pagr1a*$^{-/-}$ embryos have reduced expression of BMP2, a known regulator of extraembryonic development.

Conclusions—Loss of mouse *Pagr1a* function leads to defective extraembryonic development, likely due at least in part to altered BMP signaling, contributing to developmental arrest.

Keywords

chorion; amnion; amniochorionic fold; BMP signaling

*Correspondence to: Michael R. Kuehn, NCI-Frederick, Bldg. 560, Room 12-90, Frederick, MD 21702. mkuehn@mail.nih.gov.
‡Dr. Kumar's present address is Cancer and Developmental Biology Laboratory, National Cancer Institute, National Institutes of Health, Frederick, Maryland

Introduction

The mammalian embryo depends on extraembryonic tissues, including the placenta and the visceral yolk sac (VYS) and amnion, for intrauterine growth and survival. The amnion is the extraembryonic membrane closest to the embryo, defining the amniotic cavity and primarily playing a protective role. The VYS mediates the absorption of oxygen and nutrients from the maternal environment and their transfer to the embryo at early stages of development. The chorioallantoic placenta then assumes this function as the embryo grows larger and develops a circulatory system. The VYS is also the initial site of hematopoiesis and blood vessel formation.

Development of the extraembryonic membranes begins at gastrulation, accompanying the dynamic changes taking place in the embryonic region that result in germ layer formation and patterning. Before gastrulation, the mouse embryo is cylindrical in shape with embryonic and extraembryonic regions arranged along a proximal–distal axis with respect to the mesometrium. An inner epithelial layer composed of embryonic ectoderm (or epiblast) distally and extraembryonic ectoderm (ExE) proximally is arranged around a central lumen known as the proamniotic cavity and surrounded by an outer layer of visceral endoderm (VE). At embryonic day (E) 6.5, mesoderm formation commences at the embryonic/extraembryonic junction between the inner ectoderm and outer VE, and then expands distally to form the primitive streak demarcating the posterior region of the embryo proper. In the extraembryonic region, mesodermal cells from the proximal part of the primitive streak push both ExE and epiblast derived cells into the proamniotic cavity, thereby creating the amniochorionic fold (ACF) and the nascent exocoelom (Pereira et al., 2011). The continued expansion of the ACF eventually leads to fusion with the anterior ectoderm: the ExE derived component of the ACF fuses with anterior ExE to form the chorion and create the ectoplacental cavity; the epiblast derived ACF cells fuse with anterior proximal epiblast, giving rise to the amnion and closing off the amniotic cavity. These events occur at the anterior midline at a position called the anterior separation point (ASP), because this is where the chorionic and amniotic components of the ACF lose their connection through intercalation of mesoderm (Ellington, 1987; Pereira et al., 2011). After separation, the exocoelom expands as the chorion moves away from the amnion. This enlarges the VYS and eventually eliminates the ectoplacental cavity. A secondary growth of mesoderm from the embryonic/extraembryonic boundary forms the allantois, which grows into the exocoelom ultimately meeting and fusing with the chorion to form the chorioallantoic placenta.

Gene knockout studies in mice have shown an important role for bone morphogenetic protein (BMP) signaling in extraembryonic development (Kishigami and Mishina, 2005). BMPs are secreted ligands belonging to the transforming growth factor beta (TGF-β) superfamily that activate the intracellular effector proteins Smad1, Smad5, and Smad8 to regulate target gene expression (Massague et al., 2005). *Smad1* knockout embryos show marked defects in proliferation and morphogenesis of extraembryonic tissue including over-proliferation of the chorion within the exocoelomic cavity and a shortened allantois that fails to establish connection with the placenta (Lechleider et al., 2001; Tremblay et al., 2001). *Smad5* mutants have defects in the anterior amnion, which is thickened and displays characteristics of the primitive streak (Chang et al., 1999; Bosman et al., 2006; Pereira et al.,

2012). Embryos lacking BMP4 show defects in gastrulation and in the allantois due to reduced mesoderm formation (Winnier et al., 1995). The initial study on *Bmp2* mutant embryos showed that the ACF fails to fuse anteriorly, which was attributed to deficiencies in extraembryonic mesoderm, resulting in an open proamniotic canal (Zhang and Bradley, 1996). Subsequent analyses have pointed to a more complex, heterogeneous phenotype and provided evidence for a role in the morphogenic events that lead to enclosure of the embryo in the extraembryonic membranes and proper positioning of head and heart (Goldman et al., 2009; Madabhushi and Lacy, 2011).

Human PAX-Interacting Protein 1-associated glutamate rich protein 1 (PAGR1; also known as PA1 and GAS) was identified in a complex with PAX-Interacting Protein 1 (PAXIP1; also known as PTIP) by co-immunoprecipitation and mass spectrometry (Cho et al., 2007). Both proteins were found to be associated with MLL3/MLL4-containing histone H3K4 methyltransferase complexes (Cho et al., 2007), suggesting a role in epigenetic gene regulation. In addition, PAGR1 and PAXIP1 form a separate complex independent of MLL3/MLL4 that has a role in DNA damage repair (Gong et al., 2009). PAGR1 also acts as transcriptional co-regulator of the estrogen and glucocorticoid receptors (Liang et al., 2009; Zhang et al., 2013), a function likely independent of its association with PAXIP1 or MLL3/MLL4. Thus, PAGR1 may have multiple roles in gene regulation. Here we show that the cognate mouse gene, *Pagr1a*, is expressed first within the ExE and chorion and later expands to the entire embryo. Analysis of a targeted germ line deletion reveals that although *Pagr1a*$^{-/-}$ embryos properly specify all embryonic and extraembryonic cell lineages, profound growth defects are detected as early as E8.0. The most conspicuous abnormalities are seen in extraembryonic tissues, including the accumulation of a mass of chorionic tissue at the anterior midline, within the amniotic cavity. Our analysis suggests that *Pagr1a* mutant embryos undergo abnormal ACF formation and separation at the ASP resulting in defects in both chorion and amnion. Importantly, *Pagr1a*$^{-/-}$ embryos show reduced expression of *Bmp2*, suggesting that *Pagr1a* normally regulates *Bmp2* gene expression and that the *Pagr1a* mutant phenotype is due, at least in part, to reduced BMP2 signaling.

Results and Discussion

Pagr1a Expression is Highest in the Extraembryonic and Chorionic Ectoderm

To provide insight into the in vivo function of mouse *Pagr1a*, we used whole-mount in situ hybridization (WMISH) with a full-length cDNA probe to analyze the expression pattern of *Pagr1a* mRNA in pre- and postgastrulation embryos. Expression was first detected at E5.0 to E6.0 in the extraembryonic region (Fig. 1A, arrowheads). In the prestreak (PS) to early primitive streak stage (ES), expression was readily detected in the ExE (Fig. 1B, left panel; arrowhead). The absence of any signal in control embryos following WMISH with sense strand probe (Fig. 1B, right panel) suggested that a relatively low level of *Pagr1a* expression may also be present within the epiblast at this stage (Fig. 1B, left panel; arrow), but not in the VE. In E7.5 embryos at the early allantoic bud stage (EB), *Pagr1a* mRNA was detected strongly within the chorion (Fig. 1C,D; arrowheads). Some EB-stage embryos also showed comparatively higher levels within the embryonic region (Fig. 1D, arrow), indicating an up-regulation of expression within the embryo proper occurs around this stage. By the late head

fold stage (LHF) and into early somite stages, all embryos showed expression in both the embryonic and extraembryonic regions (Fig. 1E,F). Sectioning showed that *Pagr1a* mRNA is present in all fetal cell lineages and also within the allantois, but levels are strongest in the chorion even at these stages.

Pagr1a Loss of Function Mutation is Embryonic Lethal

To understand the consequences of loss of *Pagr1a* function, mice bearing a targeted deletion of the *Pagr1a* gene (Fig. 1G; Y-W.C., J-E.L. and K.G., manuscript in preparation) were analyzed. *Pagr1a*$^{+/-}$ heterozygous mice, identified by polymerase chain reaction (PCR) genotyping (Fig. 1H), were found to be normal and fertile. Heterozygous animals were then mated to generate *Pagr1a*$^{-/-}$ homozygotes. At weaning, no homozygotes were found out of a total of 135 offspring (Table 1), suggesting the mutation is embryonic lethal. We then examined embryos at different stages of development to determine the timing of embryonic death (Table 1). At the PS stage, 5 of 24 embryos examined were genotyped as *Pagr1a*$^{-/-}$ (Fig. 1H) but none showed any abnormalities. At the ES to late streak (LS) stage, a total of 48 embryos were analyzed, of which 11 were *Pagr1a* homozygous mutants. None of these showed any phenotype. However, at the EB to late bud (LB) stages, 3 of a total of 24 *Pagr1a*$^{-/-}$ embryos showed clear defects in the amnion and ACF (Fig. 1I, right panel, arrow). At the early head fold (EHF) to LHF stages, five of seven homozygotes showed ACF defects. Of interest, the number of mutants was higher at the EB/LB stages than expected from Mendelian ratios, and lower at the EHF/LHF stages. This suggests that mutants undergo developmental delay starting around the transition from allantoic bud to head fold stages. All E8.5 and E9.5 *Pagr1a*$^{-/-}$ embryos were developmentally delayed and showed obvious defects (see below), whereas no homozygotes were found at E10.5 and later.

Analysis using WMISH revealed a lack of expression of *Pagr1a* in homozygous mutant embryos (Fig. 1I, right panel). The absence of detectable mRNA corresponding to exon 3, which is retained in the deleted allele, may be due either to lack of transcription initiation or to mRNA instability, and suggests that the mutation is a complete null.

Pagr1a Mutants Display Multiple Embryonic and Extraembryonic Defects

The abnormal phenotype detected in E8.5 and E9.5 *Pagr1a* mutant embryos included an overall reduction in size compared with wild-type (WT) embryos, failure to undergo axial rotation (embryo turning), limited anterior development and arrest at the four- to five-somite stage, as judged by WMISH analysis using the somite marker *Uncx* (Fig. 2A,B). Striking morphological abnormalities in the extraembryonic region were also apparent. In the VYS, ring-like structures were seen, giving the membrane the appearance of being cratered (Fig. 2C, arrow and inset; Fig. 2H, arrowheads). The allantois was considerably shorter in mutants, as judged by WMISH for *Foxf1* (Fig. 2D, brackets). Most notably, tissue aggregations were seen at E8.5 above the developing cranial neural folds within the amniotic cavity (Fig. 2C,E; arrowheads) and exocoelom (Fig. 2E,G). Of interest, *Paxip1* mutant mouse embryos also show abnormal aggregates within the amniotic cavity (Cho et al., 2003), suggesting the physical interaction of PAGR1 and PAXIP1 proteins may reflect a functional interaction in extraembryonic development. Histological examination of the

tissue aggregates suggested that they consist of chorionic ectoderm (Fig. 2G). Histology also revealed a thickening of the posterior amnion in mutants (Fig. 2E, arrowhead). Examination of the VYS revealed the absence of the apical vacuoles normally seen in the endoderm layer (Fig. 2F,F′). At the LB/EHF stages, structural abnormalities in the endoderm of the VYS already were evident with the apical vacuoles appearing smaller and fewer in number (Figs. 4E,E′), suggesting the transport functions of this tissue may be impaired from an early stage. Further analysis using the TUNEL (terminal deoxynucleotidyl transferase–mediated deoxyuridinetriphosphate nick end-labeling) assay (Fig. 2I) revealed significant cell death at E8.5 in the *Pagr1a*$^{-/-}$ VYS endodermal layer (Fig. 2J), as well as in allantois (Fig. 2K) and neuroectoderm (Fig. 2L). Although the cell death seen at these late stages may not be a direct consequence of loss of *Pagr1a* function, it may contribute to the limited development of these tissues in the mutant. The cell death in the VYS may also further compromise VYS-mediated gas and nutrient exchange at E8.5, thereby precipitating embryonic demise.

Pagr1a Mutants Undergo Normal Gastrulation and Germ Layer Specification

To understand the molecular basis for the *Pagr1a*$^{-/-}$ developmental defects, we carried out WMISH analysis using gene expression markers specific for embryonic and extraembryonic lineages, examining stages both before and after the appearance of overt defects. During gastrulation, *Hoxb1* marks mesoderm arising posteriorly from the primitive streak (Fig. 3A, left panel, bracket). There was no apparent difference in *Hoxb1* expression in similarly staged *Pagr1a*$^{-/-}$ embryos (Fig. 3A, right panel). *Eomesodermin* (*Eomes*), which is essential for specification of the definitive endoderm (DE) lineage, also is expressed in mesoderm arising from the primitive streak (Fig. 3B, left panel, arrow) as well as throughout the proximal ExE (Fig. 3B, left panel, bracket). We could not detect any significant difference in *Eomes* expression in *Pagr1a*$^{-/-}$ embryos (Fig. 3B, right panel). The anterior visceral endoderm (AVE) is a population of extraembryonic cells that migrate from a distal location to the prospective anterior of the embryo. In LS/OB-stage embryos, *Cer1* is found in the AVE (Fig. 3C, left panel, arrowhead) as well as in the nascent DE (Fig. 3C, left panel, arrow). In *Pagr1a*$^{-/-}$ embryos, *Cer1* expression was similar to WT (Fig. 3C, right panel). *Nephrocan* (*Nepn*) marks the entire midgut endoderm at early somite stages (Fig. 3D, left panel, bracket). In *Pagr1a*$^{-/-}$ mutants, *Nepn* was expressed and found in the appropriate region (Fig. 3D, right panel, bracket), with the domain smaller but proportionate to that of the more developmentally advanced and larger WT littermate. Taken together these data indicate that *Pagr1a*$^{-/-}$ embryos initiate normal gastrulation and properly specify the mesodermal and endodermal lineages.

Pagr1a$^{-/-}$ embryos arrest by early somite stages, and fail to elongate along the anterior–posterior (AP) axis and to undergo embryo turning. Wnt and fibroblast growth factor signaling in the primitive streak and presomitic mesoderm (PSM) have been implicated in somite formation and AP axis elongation (Naiche et al., 2011; Pourquie, 2011). The T box transcription factors *T/Brachyury* and *Tbx6* are direct targets of Wnt signaling in the primitive streak and PSM. In E8.5 *Pagr1a*$^{-/-}$ embryos, expression levels of both markers were not significantly different from WT embryos (Fig. 3E,F; brackets). *T/Brachyury* expression in the node (Fig. 3F, arrowheads) and notochord (Fig. 3F, arrows) of *Pagr1a*$^{-/-}$ embryos also was similar to WT. These results indicate normal PSM specification and

midline patterning in *Pagr1a*$^{-/-}$ embryos, and suggest that the failure to undergo axial elongation and rotation may be a consequence of concurrent developmental arrest due to extraembryonic defects.

To analyze neural development, we first looked at *Hoxb1* in E8.5 embryos. WT embryos show expression of *Hoxb1* in rhombomere 4 (Fig. 3G, arrow). A similar domain, proportionately sized, was seen in *Pagr1a* mutant embryos suggesting proper patterning of the hindbrain. However, in more anterior domains there was altered expression of forebrain markers. Expression of *Otx2*, which marks the anterior neuroectoderm, and of *Six3*, present in the most rostral neuroectoderm, was either reduced or absent in some *Pagr1a*$^{-/-}$ embryos (Fig. 3H,I). Of interest, while the pattern of *Sox2* expression was similar to WT embryos at EB/LB stages (Fig. 3J), later-stage mutants failed to show the robust anterior expression that is found in WT embryos (Fig. 3K, brackets). This may either be the consequence of the cell death occurring in the neuroectoderm of the mutant (Fig. 2L) or point to a role for *Pagr1a* in maintaining anterior *Sox2* expression, perhaps involving epigenetic mechanisms in conjunction with MLL3/4.

Defective Formation and Resolution of the ACF in *Pagr1a* Mutants

In addition to being expressed in the embryo proper, *Sox2* marks the ExE and chorionic ectoderm (Fig. 3J, left panel, bracket). At the EB/LB stage, *Pagr1a*$^{-/-}$ embryos show an apparently normal pattern and level of Sox2 expression in the extraembryonic domain (Fig. 3J, right panel). This indicates that in *Pagr1a* mutants the ACF forms and expands toward the anterior side. However, in some mutants the proamniotic canal (PAC) appeared wider (Fig. 3J, arrows) and a distinct ruffling could be seen in the region of the forming amnion (Fig. 3J, right panel, arrowhead). To further explore these defects, we analyzed *Cldn3*, which is expressed specifically in the ExE and chorionic ectoderm from an early stage and marks the nascent ACF (Fig. 4A). In LB/EHF- and LHF-stage WT embryos, the chorionic membrane marked by *Cldn3* has separated from the amnion and segregated away from the embryonic region (Fig. 4B,F; left panels). In mutant littermates, the *Cldn3* marked chorion was found still within the exocoelom (Fig. 4B,F; right panels). Further analysis of histological sections showed that the mutant ACF consisted of *Cldn3*-positive ExE joined to embryonic ectoderm derived amnion (Fig. 4C, right panel; Fig. 4D′), whereas in WT embryos this region is derived solely from embryonic ectoderm (Fig. 4C, left panel; Fig. 4D). At later stages, *Cldn3* was found to mark the large ectopic tissue masses seen in mutants (Fig. 4F,I; right panels). Further analysis by histological sectioning confirmed that the masses consisted of *Cldn3*-positive ExE cells contiguous with amnion (Figs. 4G,H,J).

Together, these results suggest a specific order of events leading to the observed defects in amnion and chorion formation in *Pagr1a* mutants. As illustrated in the schematic shown in Figure 5A, normally the ASP represents the junction of embryonic and extraembryonic ectodermal components of the ACF to their cognate anterior tissues (Fig. 5A, left and middle panels). Subsequent separation leads to an amnion and chorion composed exclusively of embryonic ectoderm or ExE, respectively (Fig. 5A, right panel). In *Pagr1a*$^{-/-}$ embryos, there appears to be an excess or mislocalization of the ExE component of the ACF such that it extends into the embryonic domain (Fig. 5B, left panel, brackets). Thus, at the

mutant ASP there is no embryonic ectoderm, only ExE (Fig. 5B, middle panel, arrowhead). Separation from this abnormal junction appears to be incomplete in places (Fig. 2G; Fig. 4F, right panel, arrowhead), but where it does occur an abnormal membrane with both chorionic and amnionic components is formed (Fig. 5B, right panel, arrow; Fig. 4D′, arrow). It is likely that the large *Cldn3*-positive tissue masses seen at later stages in mutants result from continued proliferation of the chorionic component of this abnormal membrane.

Down-regulation of BMP2 in *Pagr1a*$^{-/-}$ Mutant Embryos

Defective extraembryonic development is a prominent feature of embryos with mutations in components of the BMP signaling pathway. Defects specific to the amnion and chorion are seen in *Smad1*, *Smad5*, and *Bmp2* mutant embryos. *Smad1* mutants show over-proliferation of the ExE resulting in excessive folding of the chorion (Lechleider et al., 2001; Tremblay et al., 2001), somewhat similar to *Pagr1a* mutants. *Smad5* mutants show extraembryonic tissue aggregates composed of mesodermal and ectodermal components of the amnion, thought to be in part due to ectopic BMP signaling (Bosman et al., 2006). These aggregates have a similar location as those seen in *Pagr1a*$^{-/-}$ embryos. However, it is not clear if they also have a chorion component, as no specific ExE markers were checked. In *Bmp2* null embryos, amnion formation is disrupted and can lead to failure to close the PAC and growth of the heart outside the amnion (Zhang and Bradley, 1996; Madabhushi and Lacy, 2011). These defects are more severe than seen in *Pagr1a*$^{-/-}$ embryos, although other phenotypic features are shared with *Pagr1a* mutants including defects in anterior development and lack of axial rotation. *Bmp2* expression is found in the mesoderm of the amnion and chorion at LS to EB stages in WT embryos (Fig. 6A,B; left panels, brackets). Of interest, in the majority of *Pagr1a*$^{-/-}$ embryos analyzed at these stages, we found either a considerable reduction in *Bmp2* expression (Fig. 6A, right panel) or almost complete down-regulation (Fig. 6B, right panel). As a control, we analyzed expression of the closely related *Bmp4* gene, which is found in extraembryonic ectoderm at the PS to LS stages (Fig. 6C,D; left panels, brackets). We found no significant difference in *Bmp4* expression levels in similarly staged *Pagr1a* mutant embryos (Figs. 6C,D; right panels). These results suggest that *Pagr1a* has a specific role in maintaining normal levels of *Bmp2* gene expression, and indicate that the *Pagr1a* mutant phenotype may be due, at least in part, to reduced BMP2 signaling.

In conclusion, *Pagr1a*$^{-/-}$ embryos undergo normal germ layer specification and developmental patterning but show limited anterior development and arrest by E8.5, likely due at least in part to defects in extraembryonic tissues that compromise their support functions. Consistent with initial *Pagr1a* expression being highest in the ExE, the first overt defects are found in the developing chorion and amnion, which derive from the ExE. *Pagr1a* is then broadly expressed in the embryonic and extraembryonic domains, and it will be an important avenue of further research to use tissue specific conditional inactivation to assess how loss of *Pagr1a* function in each lineage contributes to the phenotypic defects and embryonic arrest. Although our data shows that loss of *Pagr1a* affects *Bmp2* transcription, further studies will be required to determine if regulation is direct. For instance, it will be of interest to assess whether this involves recruitment of MLL3/MLL4 complexes to the *Bmp2* locus, or some other transcriptional co-regulatory function, as seen for ER target genes

(Liang et al., 2009). It is also possible that *Pagr1a* regulates other, still unidentified target genes that act in parallel with the BMP pathway in extraembryonic development.

Experimental Procedures

Mouse and Embryo Analysis

The *Pagr1a* deleted allele (Fig. 1G) was PCR genotyped using forward primer A located 500 bp upstream of exon 1 (5′-CAGGACCAAAGTTCCCAGCTGCAGG-3′) and reverse primer C located in exon 3 (5′-GGCCCTCTGAGTCTAAGCTGAAG-3′), which results in a 297 bp product (Fig. 1H). The WT allele was PCR genotyped using forward primer B located in intron 2 (5′-TCTCGCAGCC GGCCAAGCCAACAG-3′) and reverse primer C, which results in a 530 bp product (Fig. 1H). *Pagr1a* heterozygous animals on mixed 129S6 and C57Bl6 background were intercrossed and the day of plug detection was assigned as E0.5. Embryos were dissected in phosphate buffered saline with 0.1% Tween (PBS-T) and fixed in 4% paraformaldehyde (PFA) overnight at 4°C. After washing twice with PBS, they were dehydrated and stored in 100% methanol at −20°C. To make the *Pagr1a* probe for WMISH analysis, a full-length cDNA was obtained from Open Biosystems (clone ID 3485982) and transferred into the pCMV-SPORT6 vector. Anti-sense probe was made by restriction digestion with *Eco*RI followed by transcription with T7 polymerase. Sense strand probe was made by restriction digestion with *Hin*dIII, and transcription with SP6 polymerase. WMISH to detect expression of *Pagr1a* and other genes was done as described previously (Kumar et al., 2008). Following WMISH, selected embryos were transferred into 80% glycerol in PBS and imaged using a Leica MZ16 stereomicroscope and Zeiss AxioCam MRc5 camera with AxioVision software. Embryos were PCR genotyped postanalysis by lysing in a small volume (20 μl for E6.5, 50 μl for E7.5 and 200 μl for E8.5) of 1× GeneAmp PCR Buffer II (Applied Biosystems, N8080010) containing 0.45% NP40 and 100 μg/ml of Proteinase K, incubating at 56°C for 4 hr and then heating at 95°C for 10 min. 1 μl of the lysate was used for PCR with AmpliTaq DNA polymerase (Applied Biosystems, N8080161) using the primers and conditions for amplification described above. Selected embryos were paraffin embedded, sectioned at 5 μm and counterstained with nuclear fast red or neutral red. High-resolution images of selected sections were obtained using the Aperio Scanscope slide scanner at 40× and analyzed using Aperio Imagescope software. For immunohistochemistry, fixed embryos were dehydrated in an ethanol series, embedded in paraffin and sectioned at 8 μm. TUNEL assay was done using Apoptag peroxidase in situ apoptosis detection kit (Millipore).

Ethics Statement

All experiments involving the use of animals were carried out on approved protocols in accordance with the policies and procedures set forth by the Animal Care and Use Committees of the NCI-Frederick and the NIDDK, NIH.

Acknowledgments

We thank Jennifer Matta and Lawrence Sternberg, Histopathology lab, Leidos Biomedical Research Inc. for assistance in embryo sectioning and scanning; Naiche Adler, Mark Lewandoski and Alan Perantoni for comments on the manuscript; An Zwijsen, for helpful suggestions; Janet Rossant, Pamela Hoodless, Leif Lundh, Yuji

Mishina, Shankar Srinivas, Terry Yamaguchi, and Minoru Ko for providing plasmids for RNA probes. This work was supported in part by the Intramural Research Program of the NCI (M.R.K.) and NIDDK (K.G.).

References

Bosman EA, Lawson KA, Debruyn J, Beek L, Francis A, Schoonjans L, Huylebroeck D, Zwijsen A. Smad5 determines murine amnion fate through the control of bone morphogenetic protein expression and signalling levels. Development. 2006; 133:3399–3409. [PubMed: 16887830]

Chang H, Huylebroeck D, Verschueren K, Guo Q, Matzuk MM, Zwijsen A. Smad5 knockout mice die at mid-gestation due to multiple embryonic and extraembryonic defects. Development. 1999; 126:1631–1642. [PubMed: 10079226]

Cho EA, Prindle MJ, Dressler GR. BRCT domain-containing protein PTIP is essential for progression through mitosis. Mol Cell Biol. 2003; 23:1666–1673. [PubMed: 12588986]

Cho YW, Hong T, Hong S, Guo H, Yu H, Kim D, Guszczynski T, Dressler GR, Copeland TD, Kalkum M, Ge K. PTIP associates with MLL3- and MLL4-containing histone H3 lysine 4 methyltransferase complex. J Biol Chem. 2007; 282:20395–20406. [PubMed: 17500065]

Ellington SK. A morphological study of the development of the chorion of rat embryos. J Anat. 1987; 150:247–263. [PubMed: 3654338]

Goldman DC, Donley N, Christian JL. Genetic interaction between Bmp2 and Bmp4 reveals shared functions during multiple aspects of mouse organogenesis. Mech Dev. 2009; 126:117–127. [PubMed: 19116164]

Gong Z, Cho YW, Kim JE, Ge K, Chen J. Accumulation of Pax2 transactivation domain interaction protein (PTIP) at sites of DNA breaks via RNF8-dependent pathway is required for cell survival after DNA damage. J Biol Chem. 2009; 284:7284–7293. [PubMed: 19124460]

Kishigami S, Mishina Y. BMP signaling and early embryonic patterning. Cytokine Growth Factor Rev. 2005; 16:265–278. [PubMed: 15871922]

Kumar A, Lualdi M, Lewandoski M, Kuehn MR. Broad mesodermal and endodermal deletion of Nodal at postgastrulation stages results solely in left/right axial defects. Dev Dyn. 2008; 237:3591–3601. [PubMed: 18773491]

Lechleider RJ, Ryan JL, Garrett L, Eng C, Deng C, Wynshaw-Boris A, Roberts AB. Targeted mutagenesis of Smad1 reveals an essential role in chorioallantoic fusion. Dev Biol. 2001; 240:157–167. [PubMed: 11784053]

Liang J, Zhang H, Zhang Y, Shang Y. GAS, a new glutamate-rich protein, interacts differentially with SRCs and is involved in oestrogen receptor function. EMBO Rep. 2009; 10:51–57. [PubMed: 19039327]

Madabhushi M, Lacy E. Anterior visceral endoderm directs ventral morphogenesis and placement of head and heart via BMP2 expression. Dev Cell. 2011; 21:907–919. [PubMed: 22075149]

Massague J, Seoane J, Wotton D. Smad transcription factors. Genes Dev. 2005; 19:2783–2810. [PubMed: 16322555]

Naiche LA, Holder N, Lewandoski M. FGF4 and FGF8 comprise the wavefront activity that controls somitogenesis. Proc Natl Acad Sci U S A. 2011; 108:4018–4023. [PubMed: 21368122]

Pereira PN, Dobreva MP, Graham L, Huylebroeck D, Lawson KA, Zwijsen AN. Amnion formation in the mouse embryo: the single amniochorionic fold model. BMC Dev Biol. 2011; 11:48. [PubMed: 21806820]

Pereira PN, Dobreva MP, Maas E, Cornelis FM, Moya IM, Umans L, Verfaillie CM, Camus A, de Sousa Lopes SM, Huylebroeck D, Zwijsen A. Antagonism of Nodal signaling by BMP/Smad5 prevents ectopic primitive streak formation in the mouse amnion. Development. 2012; 139:3343–3354. [PubMed: 22912414]

Pourquie O. Vertebrate segmentation: from cyclic gene networks to scoliosis. Cell. 2011; 145:650–663. [PubMed: 21620133]

Tremblay KD, Dunn NR, Robertson EJ. Mouse embryos lacking Smad1 signals display defects in extra-embryonic tissues and germ cell formation. Development. 2001; 128:3609–3621. [PubMed: 11566864]

Winnier G, Blessing M, Labosky PA, Hogan BL. Bone morphogenetic protein-4 is required for mesoderm formation and patterning in the mouse. Genes Dev. 1995; 9:2105–2116. [PubMed: 7657163]

Zhang H, Bradley A. Mice deficient for BMP2 are nonviable and have defects in amnion/chorion and cardiac development. Development. 1996; 122:2977–2986. [PubMed: 8898212]

Zhang Z, Sun Y, Cho YW, Chow CC, Simons SS Jr. PA1 protein, a new competitive decelerator acting at more than one step to impede glucocorticoid receptor-mediated transactivation. J Biol Chem. 2013; 288:42–58. [PubMed: 23161582]

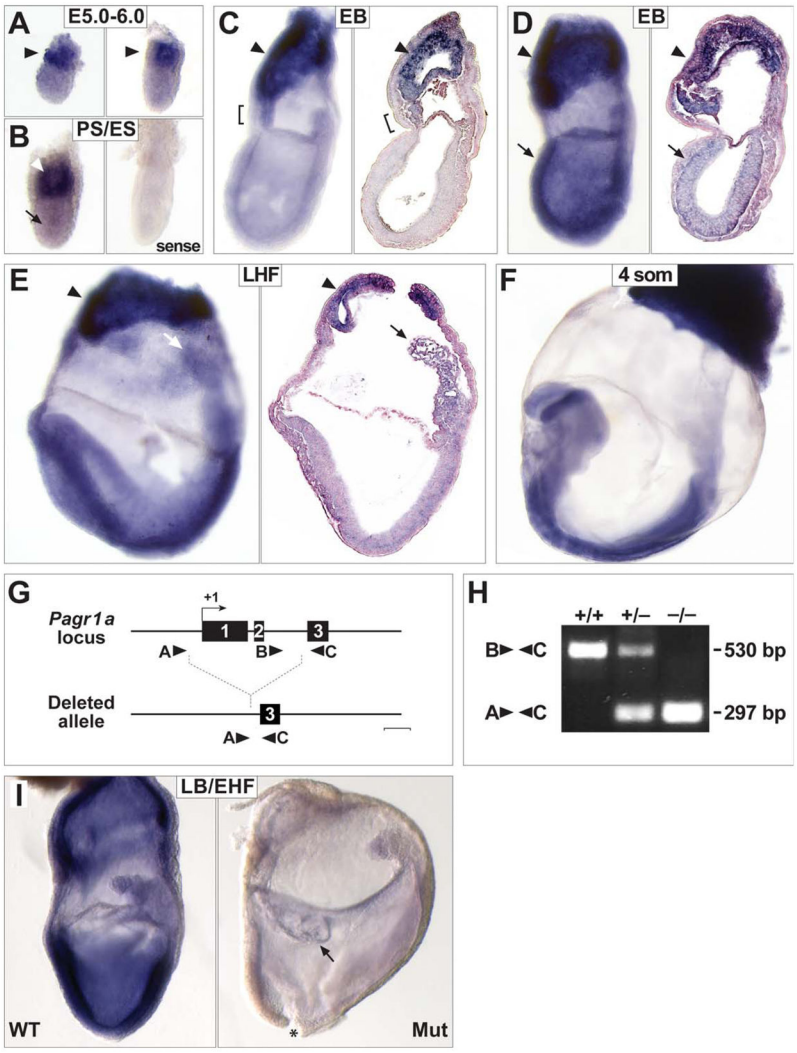

Fig. 1.

Expression pattern and targeted mutation of the mouse *Pagr1a* locus. **A:** WMISH analysis at E5.0 to E6.0 showing expression of *Pagr1a* mRNA specifically in the extraembryonic region (arrowheads). **B:** The left panel shows WMISH analysis of a PS/ES-stage embryo with *Pagr1a* expression in the ExE (arrowhead). The right panel shows analysis of a PS/ES-stage embryo using sense strand probe. The lack of any signal suggests that the faint staining seen in the epiblast of the embryo to the left (arrow) represents low-level *Pagr1a* expression. **C:** WMISH analysis and mid-sagittal section of an EB-stage embryo showing strong *Pagr1a* expression in chorionic ectoderm (arrowheads). The chorion is still in contact with the amnion (brackets). **D:** WMISH and mid-sagittal section of another EB-stage embryo, showing strong expression of *Pagr1a* in the chorion (arrowheads) and also in the embryonic region (arrows). **E:** WMISH and mid-sagittal section of a LHF-stage embryo. *Pagr1a* is strongest in the chorion (arrowheads) but is also seen throughout the embryonic region and in the allantois (arrows). **F:** WMISH analysis of a four-somite–stage (4 som) embryo with ubiquitous *Pagr1a* expression. **G:** Schematic representation of the mouse *Pagr1a* genomic locus and targeted deleted allele. The *Pagr1a* gene contains three exons, represented by the

three black rectangles. The deleted allele lacks the region containing exons 1 and 2. **H:** PCR genotype analysis of genomic DNA prepared from WT (+/+) heterozygous (+/−) and homozygous mutants (−/−). The arrowheads in (G) indicate location of primers used for genotyping the WT and deleted alleles. bp, base pairs. **I:** WMISH analysis of *Pagr1a* expression in a LB/EHF-stage WT embryo and *Pagr1a*$^{-/-}$ mutant (Mut) littermate. No expression is seen in the mutant suggesting the deletion results in complete loss of function. The arrow points to the abnormal amnion and the asterisk marks tissue damage arising during dissection.

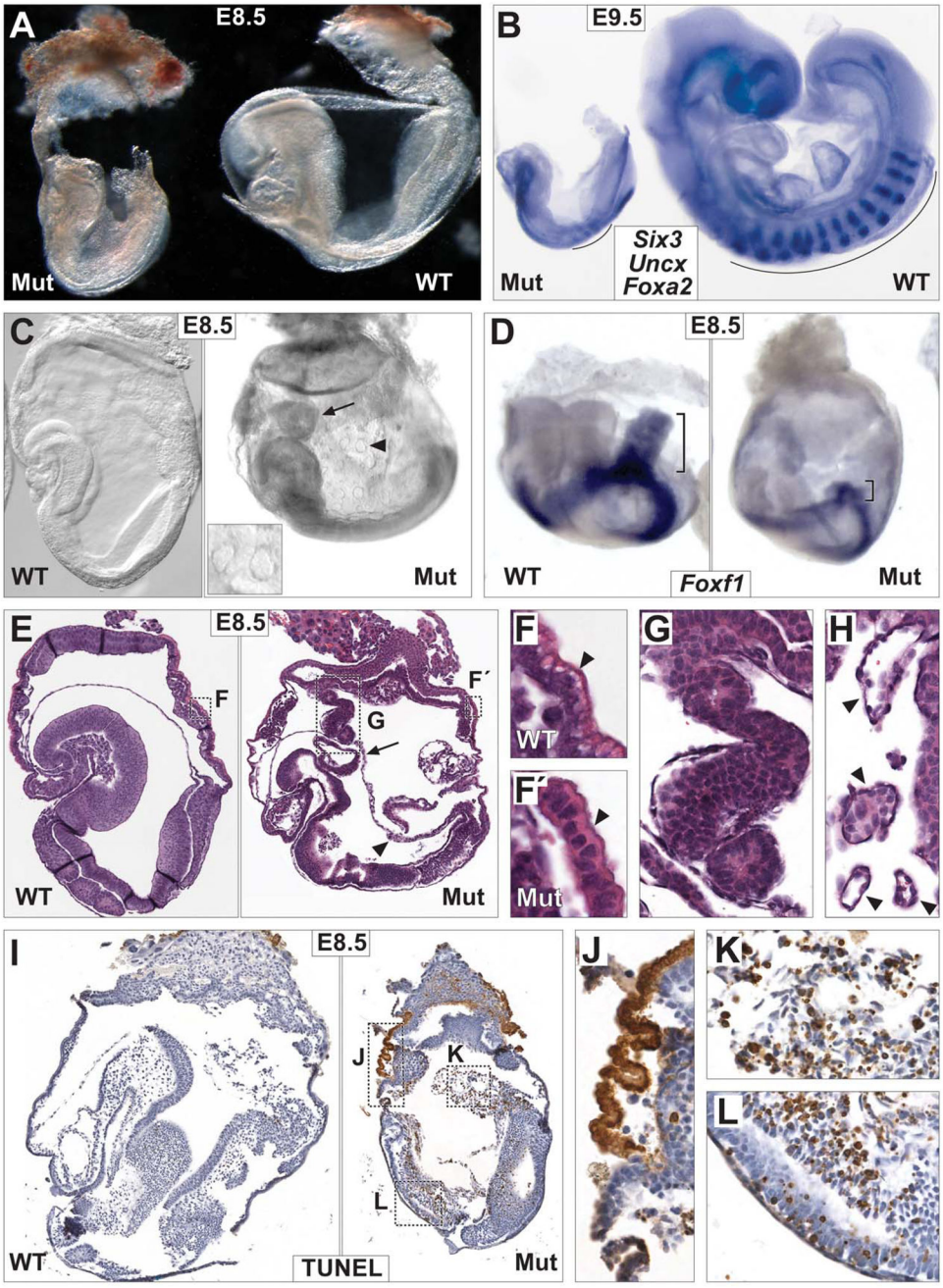

Fig. 2.

Pagr1a$^{-/-}$ embryos exhibit severe growth defects and extraembryonic abnormalities. **A:** Lateral views of an E8.5 WT embryo (right) and mutant littermate (left) showing significant growth retardation. Anterior is to the left. **B:** Lateral views of an E9.5 WT embryo (right) and mutant littermate (left) after WMISH with a probe for the somite marker *Uncx*, the midline marker *Foxa2* and the forebrain marker *Six3*. The WT littermate has 13 to 14 somites, whereas only 3 to 4 somites are detected in the mutant (curved lines). In addition, the WT embryo has undergone axial rotation while the mutant is unturned. **C:** Lateral views of an E8.5 WT embryo and similarly staged mutant embryo. Anterior is to the left. The

mutant has an ectopic tissue mass (arrow) and abnormal VYS with crater-like structures (arrowhead). Inset shows cratering of the VYS at higher magnification. **D:** Posterior views of an E8.5 WT embryo and mutant littermate after WMISH with a probe for *Foxf1*, which marks lateral plate mesoderm and allantois (bracket). Only limited allantoic growth is detected in the mutant (bracket). **E:** Sagittal sections of the embryos shown in (C). The ectopic tissue mass (arrow) is within the amniotic cavity. Corresponding regions of the VYS are marked by dotted rectangles and magnified in (F) and (F′). The abnormal extension of the chorion is marked by a dotted rectangle and magnified in (G). The arrowhead marks the abnormally thickened amnion in the posterior. **F:** Close up of WT VYS showing the apical vacuoles of the endoderm (arrowhead). **F′**: Close up of mutant VYS endoderm to highlight absence of apical vacuoles (arrowhead). **G:** Close up of abnormal extension of the chorion seen in the mutant. **H:** Close up of the VYS from an extreme lateral sagittal section of the mutant shown in (C) and (E) to illustrate the crater-like structures (arrowheads) in more detail. **I:** TUNEL analysis of E8.5 WT and mutant embryos. Cell death is limited in the WT but extensive in the mutant. **J–L:** Regions marked by dotted rectangles and shown in higher magnification include the VYS (J), the allantois (K), and neural tube (L).

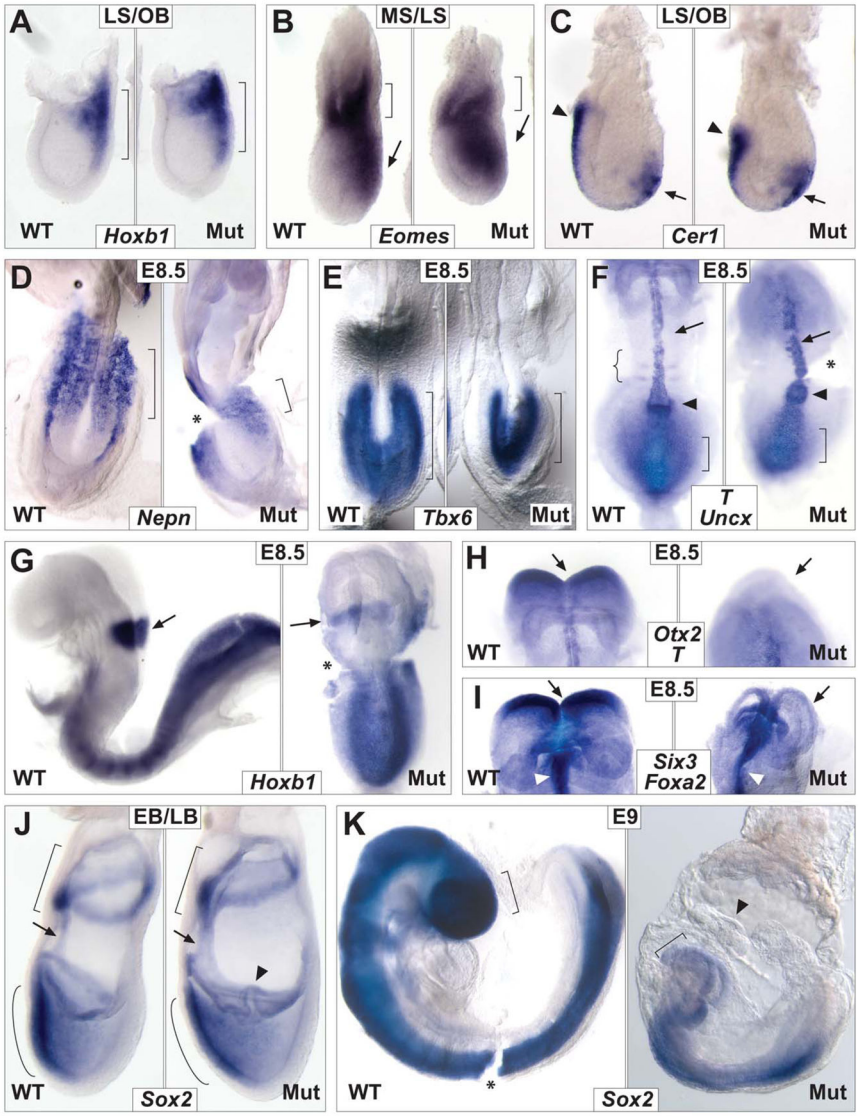

Fig. 3.

Pagr1a$^{-/-}$ embryos undergo normal gastrulation and patterning. **A:** Lateral views of WT and mutant littermates at the LS/OB stage after WMISH with a *Hoxb1* probe, which marks mesoderm arising at the posterior (brackets). There is no significant difference in expression. **B:** Lateral views of MS/LS-stage WT and mutant littermates showing no significant difference in *Eomes* expression in the primitive streak (arrows) or in the ExE (brackets). **C:** Lateral views of LS/OB-stage WT and mutant littermates showing similar *Cer1* expression in the DE (arrows) and AVE (arrowheads). **D:** Ventral views of E8.5 WT and mutant embryos after WMISH for *Nepn*, which marks the midgut endoderm (brackets). The expression domain in the mutant is proportionately sized. **E:** Ventral views of E8.5 WT and mutant littermates with presomitic mesoderm marked by *Tbx6* (brackets). The expression domain in the mutant is proportionately sized. **F:** Ventral views of E8.5 WT and mutant littermates after WMISH for *T/Brachyury* (*T*), *Uncx* and *Otx2* (not visible). Two to three somites are seen in the WT (curly bracket), but none in the mutant. Expression of *T* in

the PSM (brackets), node (arrowhead) and notochord (arrow) is similar in WT and mutant. **G:** Lateral view of an E8.75 WT embryo showing *Hoxb1* expression in rhombomere 4 in the hindbrain (arrow) and ventral view of a mutant littermate with a similar expression domain (arrow). **H:** Ventral views of the anterior-most regions of the same E8.5 WT and mutant littermate in (F) showing *Otx2* expression normally present in the forebrain is absent in the mutant (arrows). **I:** Ventral views of the anterior-most regions of an E8.5 WT and mutant littermate following WMISH for *Six3* and *Foxa2*. *Six3*, normally expressed in the forebrain, is absent in the mutant (arrows) whereas *Foxa2* midline expression is retained (arrowheads). **J:** Lateral views of EB/LB WT and mutant littermates. *Sox2* expression is seen in the anterior neuroectoderm (curves) and ExE (brackets) in both. The PAC of the mutant is wider (arrows) and the amnion is irregular (arrowhead). **K:** Lateral views of E9.0 WT and mutant littermates showing robust *Sox2* expression in the WT anterior neuroectoderm but not in the mutant (brackets). A prominent ectopic mass is seen in the mutant (arrowhead). The asterisks in (D), (F), (G), and (K) mark tissue damage arising from dissection.

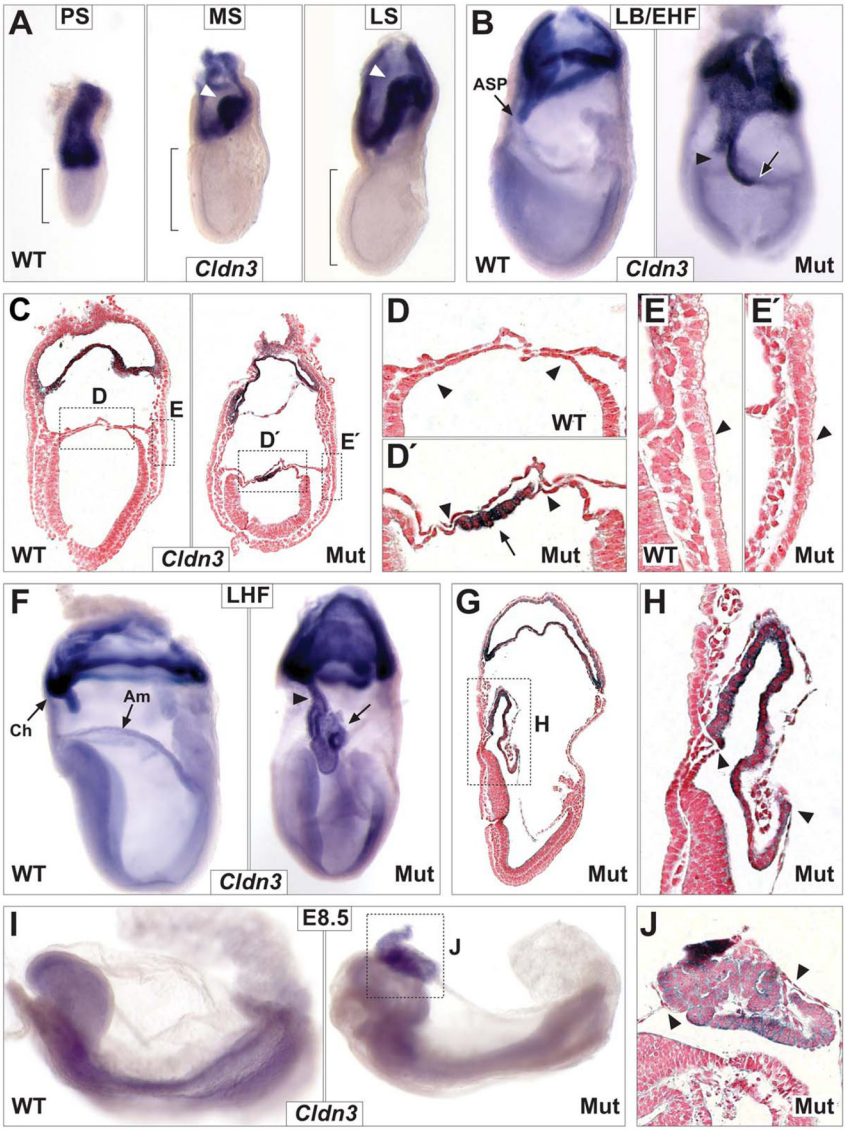

Fig. 4.

Defective formation and separation of the ACF in *Pagr1a*$^{-/-}$ embryos. **A:** Normal pattern of expression of *Cldn3* in the ExE at PS (left panel), MS (middle panel), and LS (right panel) stages. The ACF (white arrowheads) is apparent by MS. *Cldn3* is never found within the embryonic region (brackets). **B:** Lateral views of LB/EHF-stage WT and mutant littermates showing *Cldn3* expression in the chorionic ectoderm. The ACF is undergoing separation at the ASP in the WT (left panel), whereas the ACF in the mutant is aberrantly located (right panel, arrowhead) with the distal-most portion within the embryonic region (right panel, arrow). **C:** Mid-frontal sections of the WT and mutant embryos shown in (B). The amnion is outlined by dotted rectangles and shown in higher magnification in (D) and (D′). The VYS at the boundary of the embryonic and extraembryonic domains also is outlined by dotted rectangles and shown at higher magnification in (E) and (E′). **D:** Close up of the WT amnion showing continuity with the embryonic ectoderm (arrowheads). **D′**: Close up of the mutant amnion showing *Cldn3*-positive chorionic cells (arrow) continuous with the amnionic

embryonic ectoderm (arrowheads). **E:** Close up of the WT VYS showing prominent apical vacuoles within the endoderm layer (arrowhead). **E′**: Close up of the mutant VYS. The endodermal vacuoles appear smaller and fewer in number (arrowhead). **F:** Lateral views of LHF-stage WT and mutant littermates. The *Cldn3* marked chorion (Ch) has separated from the amnion (Am) in the WT, whereas a large ectopic mass is seen within the mutant exocoelom (right panel, arrow) that is connected to the chorion (right panel, arrowhead). **G:** Sagittal section of the mutant embryo shown in (F). The area containing *Cldn3*-positive cells is outlined by the dotted rectangle and shown in higher magnification in (H). **H:** Close up showing that the *Cldn3*-positive chorionic cells maintain continuity with the amnion (arrowheads). **I:** Lateral views of E8.5 WT and mutant littermates after WMISH with *Cldn3*. A large ectopic mass is seen above the head of the mutant. This mutant was sagittally sectioned with the area defined by the dotted rectangle shown in higher magnification in (J). **J:** The large ectopic mass seen in the mutant in (I) is *Cldn3*-positive and in continuity with the amnion (arrowheads).

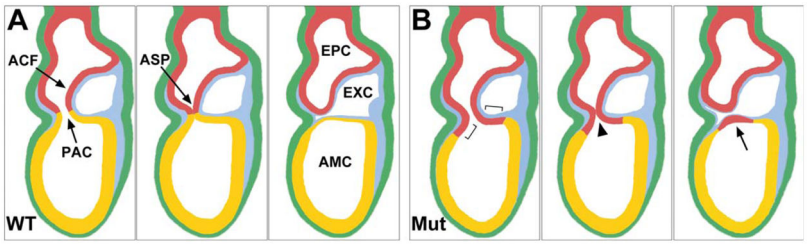

Fig. 5.

A: Schematic representation of normal amnion and chorion formation from the ACF. Yellow, embryonic ectoderm; red, ExE; blue, mesoderm; green, endoderm. PAC, proamniotic canal; EPC, ectoplacental cavity; EXC, exocoelom; AMC, amniotic cavity. **B:** Schematic representation of amnion and chorion formation in the mutant. There is excess ExE within the ACF (brackets) such that the ASP contains only ExE (arrowhead). Following separation there is ExE derived tissue within the amnion (arrow).

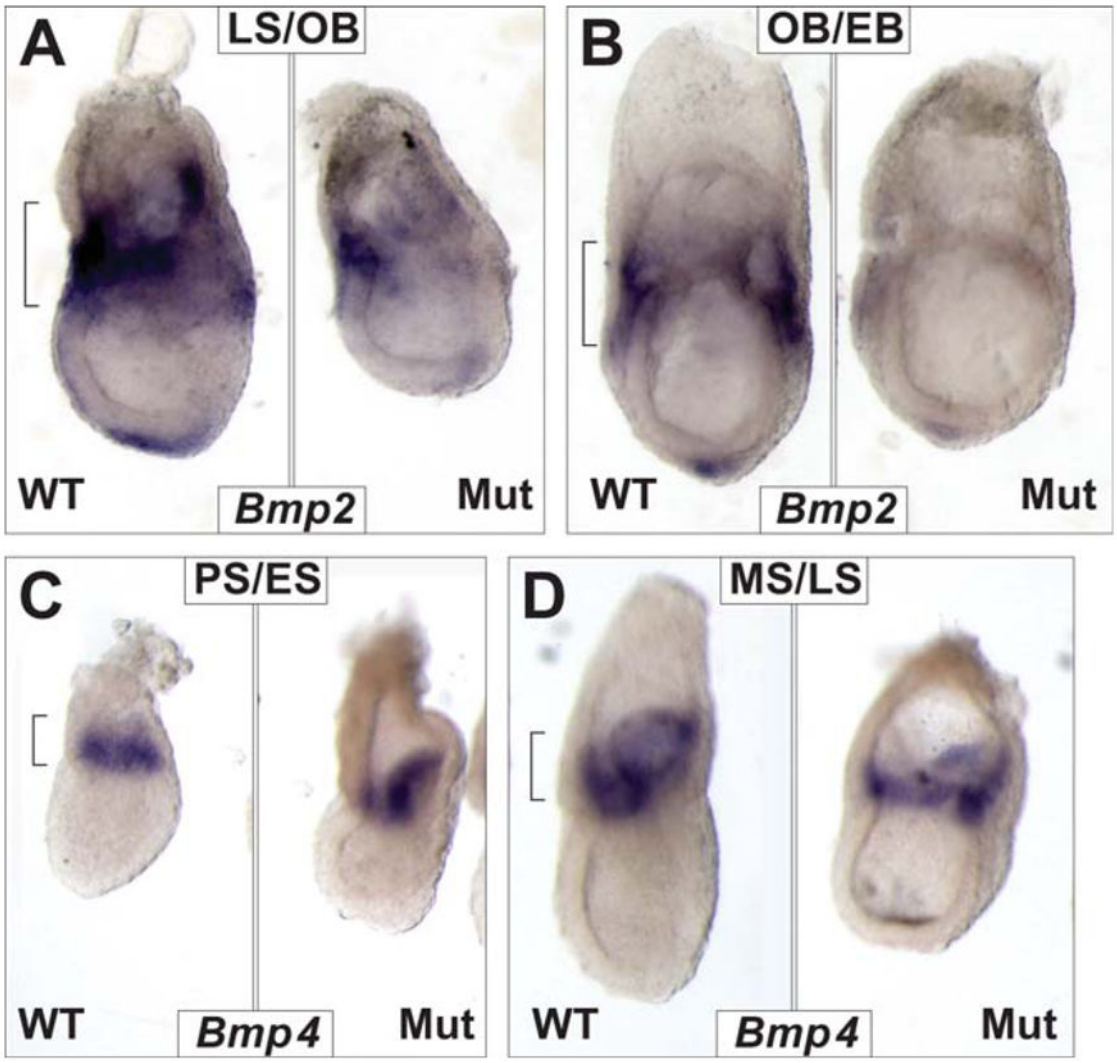

Fig. 6.

Down-regulation of *Bmp2* gene expression in *Pagr1a*$^{-/-}$ embryos. **A:** Lateral views of LS/OB-stage WT and mutant littermates showing *Bmp2* expression in the mesoderm of the amnion and chorion (bracket) is significantly reduced in the mutant. **B:** Frontal views of OB/EB-stage WT and mutant littermates showing loss of *Bmp2* expression in the mutant. **C:** Lateral views of PS/ES-stage WT and mutant littermates showing no significant difference in expression of *Bmp4* in the proximal ExE (bracket). **D:** Lateral views of MS/LS-stage WT and mutant littermates also showing no apparent change in *Bmp4* expression (bracket).

TABLE 1

Phenotypic analysis of *Pagr1a* mutant embryos

Stage	No. examined	No. *Pagr1a*$^{-/-}$	No. abnormal
PS	24	5 (21%)	0
ES/LS	48	11 (22%)	0
EB/LB	66	24 (37%)	3[a]
EHF/LHF	59	7 (11%)	5[b]
E8.5	111	27 (24%)	27[c]
E9.5	64	17 (27%)	17[d]
E10.5	23	0	–
E13.5	85	0	–
Pups	135	0	–

[a] Amnion ruffled.

[b] ACF not resolved into amnion and chorion.

[c] 4 mutants still at LHF, 23 at 0–4 somites; all with ACF defects. WT at 3–11 somites.

[d] All mutants<5 somites, none turned; all WT with >13 somites, all turned.